Vibrational spectroscopy and aromaticity investigation of squarate salts: A theoretical and experimental approach

ARTICLE *in* JOURNAL OF MOLECULAR STRUCTURE · AUGUST 2006

Impact Factor: 1.6 · DOI: 10.1016/j.molstruc.2006.01.035

PCCP

Theoretical analysis of the oxocarbons: The solvent and counter-ion effects on the structure and spectroscopic properties of the squarate ion

Georgia M. A. Junqueira,[ac] Willian R. Rocha,[b] Wagner B. De Almeida[c] and Hélio F. Dos Santos*[a]

[a] *NEQC: Núcleo de Estudos em Química Computacional, Departamento de Química, ICE, Universidade Federal de Juiz de Fora, Campus Martelos, CEP 36036-330, Juiz de Fora, MG, Brazil. E-mail: helius@quimica.ufjf.br; Fax: +55 32 3229 33 14*

[b] *Departamento de Química Fundamental, CCEN, Universidade Federal de Pernambuco, Cidade Universitária, CEP 50740-901, Recife, PE, Brazil*

[c] *LQC-MM: Laboratório de Química Computacional e Modelagem Molecular, Departamento de Química, ICEx, Universidade Federal de Minas Gerais, Campus Pampulha, CEP 31270-901, Belo Horizonte, MG, Brazil*

Received 7th October 2002, Accepted 5th December 2002
First published as an Advance Article on the web 23rd December 2002

The squarate anion and their coordination compounds with Li^+, Na^+ and K^+ are studied in gas phase and aqueous solution using *ab initio* quantum chemical methods and a sequential Monte Carlo/quantum mechanical procedure. The infrared and Raman spectra were calculated and the vibrational modes assigned at the second order Møller–Plesset perturbation (MP2) level of theory, employing standard split-valence basis set with inclusion of polarization and diffuse functions (6-31G(d), 6-31+G(d), 6-311+G(d), 6-311+G(2d), 6-311+G(2df)) on the O and C atoms. The vibrational analysis showed an important role played by the polarization functions on the low frequency vibrations. The solvent and counter-ions effects on the electronic spectrum are analyzed showing that both should be included in the calculation in order to reproduce the observed UV spectrum. This conclusion supports our previous analysis on the oxocarbon series.

Introduction

Oxocarbons are molecules with general formula $(C_nO_n)^{2-}$ first identified by West as a new class of aromatic compounds.[1] The main dianion oxocarbon representatives are rhodizonate ($n = 6$), croconate ($n = 5$), squarate ($n = 4$) and deltate ($n = 3$) (Fig. 1). Their structures are planar with D_{nh} symmetry, as was proposed from Raman and infrared (IR) spectroscopic analysis[2–6] and confirmed by X-ray diffraction studies.[7–10] The electronic structure of the oxocarbons has raised some questions about the aromaticity of these compounds, and there are some works in the literature dealing with this interesting property.[11,12] The general conclusion is that the aromaticity decreases with the ring size.[12] Due to the high degree of electronic delocalization, the oxocarbon ions present a strong absorption in the UV and visible regions. A peculiar and interesting aspect concerning the electronic spectrum of this class of molecule in solution is the presence of two absorption bands that have been attributed to the Jahn–Teller effect on the first singlet electronic excited state.[13]

Despite the extensive literature on oxocarbons,[14] theoretical studies are sparse.[15–19] In our previous papers[20–22] we have analyzed the structure and spectroscopic properties of the croconate and deltate ions in the gas phase and aqueous solution using quantum mechanical *ab initio* methods and Monte Carlo simulation. The main conclusion drawn was that the solvent and counter-ion effects are important to reproduce the observed electronic spectra of the oxocarbon anions in solution.[20–22] In the present study, we extend our theoretical proposal described in references[20–22] to the squarate ion. Within the oxocarbons series, the squarate derivative has been extensively studied.[23] This oxocarbon anion and its derivatives exhibit many applications due to their photochemical and photoconductive properties as electron acceptors for nonlinear optical materials.[24] In addition to the overall solvent effect analyzed for the croconate derivative[20] and the detailed analysis of the hydrogen bond effect on the electronic spectrum of the deltate derivative,[21] in the present paper we also investigated the effect of the different counter-ions, Li^+, Na^+ and K^+, on the electronic spectrum of the squarate anion.

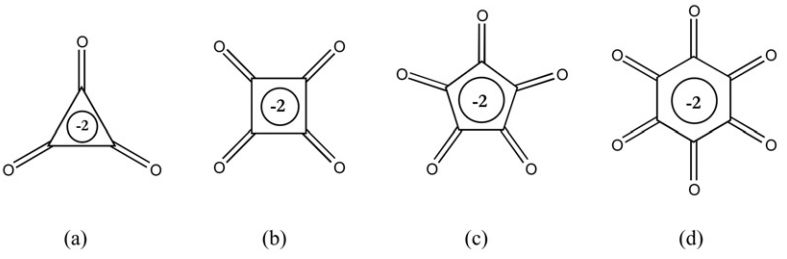

Fig. 1 Cyclic oxocarbon ions. (a) deltate, (b) squarate, (c) croconate and (d) rhodizonate.

Theoretical methodology

Gas phase

The geometry of the squarate ion was fully optimized in gas phase at the Møller–Plesset second order perturbation (MP2) level of theory, employing standard split-valence basis-sets with inclusion of polarization and diffuse functions (6-31G(d), 6-31+G(d), 6-311+G(d), 6-311+G(2d), 6-311+G(2df))[25] on the O and C atoms.

The vibrational frequencies, infrared intensities and Raman activities were obtained for the $(C_4O_4)^{2-}$ anion at each level of calculation mentioned before. The electronic spectra in the gas phase and solution were calculated within the INDO/CIS semi-empirical approach,[26] using the MP2/6-31+G(d) optimized structures.

Aqueous solution

The solvent environment was modeled through Monte Carlo (MC) statistical mechanics simulation employing standard procedures[27] including the Metropolis sampling technique[28] and periodic boundary conditions using the minimum image method in a cubic box. The simulations were performed in the canonical (NVT) ensemble. The system under investigation consisted of one squarate anion and 499 solvent molecules (water). The volume of the cubic box was determined by the experimental density of water,[29] which is 0.9966 g cm^{-3} at $T = 298.15$ K and $p = 1$ atm. The intermolecular interactions were described by the Lennard-Jones plus Coulomb potential (eqn. (1)), with three parameters for each atom i (ε_i, σ_i and q_i).

$$U_{\text{int}} = 4\sum_{i}^{\text{on } a}\sum_{j}^{\text{on } b}\varepsilon_{ij}\left[\left(\frac{\sigma_{ij}}{r_{ij}}\right)^{12} - \left(\frac{\sigma_{ij}}{r_{ij}}\right)^{6}\right] + \frac{q_i q_j}{r_{ij}} \qquad (1)$$

The set of intermolecular parameters employed in the simulations is shown in Table 1. The σ and ε parameters were taken from the OPLS force field[30] and do not differ significantly from the OPLS force field expanded to include squaramides and squaric acid, published in a recent paper.[31] The atomic charges were obtained from the ChelpG fitting procedure[32] at the MP2/6-31+G(d) level. The intermolecular interactions were spherically truncated for a center of mass separation greater than the cutoff radius $r_C = 12.374$ Å. In all simulated systems, the molecular geometry was kept rigid. The water molecules in their C_{2v} structure with $r_{OH} = 0.9572$ Å and $\angle HOH = 104.52°$[33] and the squarate ion in its D_{4h} structure optimized at the MP2/6-31+G(d) level of theory. The initial positions and orientations of the molecules were generated randomly. Configurations for the subsequent analysis were stored after every 200 MC steps, *i.e.*, after all solvent molecules sequentially attempt to translate in all cartesian directions and also attempt to rotate around a randomly chosen axis. The maximum allowed displacement of the molecules was self-adjusted after 5000 MC steps to give an acceptance ratio of new configurations around 50%. The maximum rotation angle was fixed during the simulation in $\delta\theta = \pm 15°$. The simulations consisted of a thermalization phase of 10 000 MC steps, followed by an averaging stage of 60 000 MC steps. Thus, the total number of configurations generated from the MC simulation was 3.5×10^7.

A preferential sampling was applied in the average phase in order to improve the water moves by a factor of two in a spherical shell of approximately 6 Å from the center of mass of the solute molecule.

To analyze the solvent effect on the electronic spectrum of the solute molecule we employed a sequential Monte Carlo/Quantum mechanics procedure,[34] in which the quantum mechanical calculations are performed on super-molecular clusters, generated by the MC simulations, composed of one solute molecule and all solvent molecules within a specific solvation shell. Since we have thousands of configurations, a procedure must be applied to reduce the number of super-molecular clusters that are submitted to the quantum mechanical calculations. The configurations are selected according to the autocorrelation function of the energy[35] that has been described elsewhere.[20–22] The interval between uncorrelated configurations, the so-called correlation step τ, is calculated by performing the integration of the autocorrelation function. In general, configurations separated by 2τ, or larger, have less than 12% of statistical correlation.[35] As for the croconate and deltate derivatives, we have selected uncorrelated configurations at each 4×10^5 MC steps, giving a total of 75 nearly uncorrelated configurations to be considered in the quantum mechanical electronic spectrum calculation. The solvation shells were defined from the radial distribution functions (RDF) and the electronic spectra in aqueous solution were then calculated within the INDO/CIS semi-empirical approach.[26] As the appropriate Boltzmann weights are included in the Metropolis Monte Carlo sampling technique, the average values of the transition energies and solvatochromic shifts are given as an arithmetic average over the 75 uncorrelated configurations.

All *ab initio* calculations reported here were performed using the Gaussian/98 program[36] and the Monte Carlo statistical mechanics simulations were carried out using the DICE program.[37]

Table 1 Intermolecular parameters used in the Monte Carlo simulations (q_i/e, ε_i/kcal mol^{-1} and σ_i/Å)

Atomic site	q_i	ε_i	σ_i
H_2O[a]			
O	−0.834	0.152	3.151
H	0.417	0.000	0.000
$(C_4O_4)^{2-}$[b]			
C	0.282	0.105	3.750
O	−0.782	0.210	2.960
$[Li_2(C_4O_4)]$ (Form A)[b c]			
C(1)	0.088	0.105	3.750
C(2)	0.330	0.105	3.750
C(3)	0.330	0.105	3.750
O(1)	−0.784	0.210	2.960
O(2)	−0.671	0.210	2.960
O(3)	−0.483	0.210	2.960
Li	0.851	0.018	2.126
$[Li_2(C_4O_4)]$ (Form B)[b c]			
C	0.227	0.105	3.750
O	−0.617	0.210	2.960
Li	0.781	0.018	2.126

[a] TIP3P potential.[33] [b] OPLS parameters[30] with the charges calculated using the ChelpG fitting procedure[32] at the MP2/6-31+G(d) level of theory. [c] The optimized structure and numbering scheme are shown in Fig. 3.

Results and discussion

Structure and vibrational spectrum of the $(C_4O_4)^{2-}$ ion

The optimized structural parameters obtained for the squarate anion are reported in Table 2 for the distinct levels of theory used. In general the calculated geometries are in good agreement with the experimental data. Analyzing the values in Table 2 it can be noted that the inclusion of diffuse functions on the 6-31G(d) basis-set increases the C=O and decreases the C–C bond lengths. This effect is reverted for the triple-zeta quality basis-set (MP2/6-311+G(d)). The addition of two sets of d polarization functions does not change the geometry

Table 2 Structural parameters[a] calculated for the free squarate ion

	MP2/ 6-31G(d)	MP2/ 6-31+G(d)	MP2/ 6-31+G(2d)	MP2/ 6-311+G(d)	MP2/ 6-311+G(2d)	MP2/ 6-311+G(2df)	Expt.[b] ($K_2C_4O_4$)
C=O	1.269	1.272	1.272	1.262	1.262	1.272	1.259
C–C	1.493	1.489	1.489	1.491	1.491	1.489	1.483
∠C–C–C	90.0	90.0	90.0	90.0	90.0	90.0	82.2
∠C–C–O	135.0	135.0	135.0	135.0	135.0	135.0	134.8

[a] Bond lengths in Å and bond angle in degrees. [b] From ref. 40.

significantly. The structure obtained from our highest level MP2/6-311+G(2df) was essentially the same as that optimized at MP2/6-31+G(d) (see Table 2). The structure of the squarate ion was found to be planar with high symmetry (D_{4h}) and the vibrational frequencies of all infrared and Raman active modes have been measured.[38] The frequencies and absolute intensities are reported in Table 3. Regarding the IR spectrum of the squarate ion, seven active modes were assigned (Table 3) relative to the CO stretching (E_u), CC stretching (E_u), in plane CO bending (E_u) and out-of-plane CO deformation (A_{2u}) (see Fig. 2c for the vibrational modes representation). The B_{2u} and A_{2g} modes assigned to δ_{oop}(CO)/ν(CC) are inactive in both IR and Raman spectra (Table 3). An imaginary frequency was observed for the B_{2u} mode at 300i (MP2/6-31+G(d)) and at 41i (MP2/6-311+G(d)) assigned to ring warping (Fig. 2a). At the MP2/6-31G(d) level no imaginary frequency was observed. This is also the case found when two sets of polarization functions are included in the calculation. So, the appearance of an imaginary frequency in the calculated vibrational spectrum of squarate can be attributed to inadequacy of the basis set. Similar imaginary frequency result has been reported in ref. 19. In that paper an imaginary frequency was also observed at MP3/6-31+G(d), showing that this result does not strongly depend on the level of electronic correlation. The authors also showed that at the HF/6-31+G(df) level the frequency of the B_{2u} mode becomes real. So, analyzing the results from the present paper and from ref. 19 it can be concluded that the inclusion of polarization functions (d or f) is essential to get accurate values of low vibrational frequencies of the squarate anion. From the data in Table 3 it can be observed some disagreement between the calculated absolute and experimental relative intensities. At the MP2/6-31G(d) level the B_{2g} ν(CC) mode is assigned as very strong (vs), however its Raman activity was found to be lower than those calculated for the A_{1g} ν(CO)/ν(CC) mode, which was experimentally assigned as weak (w). At higher levels at theory this disagreement was not observed (see Table 3). For the IR active modes the experimental relative intensities are in agreement with the calculated values. In general there is a good agreement between the theoretical and experimental frequencies, with the larger average deviation (41 cm^{-1}) found at MP2/6-31G(d). The MP2/6-311+G(df) presented the best values for the vibrational frequencies of the squarate ion, with the absolute average deviation found to be only 26 cm^{-1}. From the data in Table 3 it can be seen that the inclusion of diffuse functions on the basis-set is responsible for a systematic decreasing of the frequencies relative to those calculated at MP2/6-31G(d). The absolute average deviation was 30 cm^{-1} for the calculations including diffuse and d polarization functions.

Electronic spectrum in gas phase

The computed gas phase electronic spectrum for the squarate ion showed two degenerate transitions centered at 357 nm with oscillator strength $f = 0.5$, attributed to the transitions from HOMO to LUMO and from HOMO to LUMO + 1. The experimental data for the electronic spectrum of the squarate has not been reported so far, however according to the literature two absorption bands at wavelength close to 300 nm are expected.[13] As observed for the other members of the oxocarbon series, the presence of these bands in the experimental spectrum of squarate ion should be attributed to the breaking of degeneracy due to Jahn–Teller distortions of the first electronic excited state.[13] This fact is peculiar to the species with D_{nh} symmetry.

In our previous papers,[20–22] it was shown that the inclusion of the counter ions, coordinated to the solute, and solvent molecules splits the absorption band and a blue shift is obtained relative to the gas phase transition. In order to

Table 3 Vibrational frequencies (in cm^{-1}), calculated for the free squarate ion[a]

Activity	MP2/ 6-31G(d)	MP2/ 6-31+G(d)	MP2/ 6-31+G(2d)	MP2/ 6-311+G(d)	MP2/ 6-311+G(2d)	MP2/ 6-311+G(2df)	Expt.[b]	Assignment
R	1817(82)	1787(36)	1765(20)	1790(20)	1757(15)	1792(14)	1794w	A_{1g}(ν(CO)/ν(CC))
R	1668(102)	1600(164)	1581(136)	1601(171)	1583(153)	1606(149)	1593s	B_{1g} ν(CO)
IR[c]	1649(1121)	1584(1772)	1555(1764)	1580(1842)	1547(1789)	1578(1780)	1530vs	$E_u$$\nu$(CO)
R	1050(17)	1060(58)	1038(57)	1043(59)	1030(60)	1048(59)	1123vs	B_{2g} ν(CC)
IR[c]	1089(32)	1081(13)	1069(26)	1077(20)	1068(23)	1080(21)	1090s	E_u ν(CC)
R	693(52)	692(58)	682(55)	690(54)	680(54)	691(52)	723s	A_{1g} ring breathing
R[c]	650(0)	611(7)	660(8)	640(7)	656(6)	670(6)	662vw	E_g δ_{oop}(CO)
R	620(32)	622(40)	620(39)	622(39)	622(39)	627(37)	647s	B_{1g} ν(CC)
IR[c]	309(3)	316(4)	313(5)	315(4)	315(5)	319(5)	350m	E_u δ(CO)
R	251(10)	265(11)	263(11)	263(13)	266(12)	267(11)	294w	B_{2g} δ(CO)
IR	257(27)	223(23)	239(21)	229(22)	237(22)	241(23)	259s	A_{2u} δ_{oop}(CO)
ia[d]	838	830	834	831	839	844	—	A_{2g} δ_{oop}(ν(CO)/ν(CC))
ia	251	175	687	418	701	725	—	B_{2u} δ_{oop}(ν(CO)/ν(CC))
ia	79	300i	91	41i	100	99	—	B_{2u} ring warp

[a] IR and R stand for InfraRed and Raman, respectively. Intensities are given in parenthesis in units of km mol^{-1} and $Å^4$ u^{-1} for the IR and R active modes, respectively. [b] From ref. 38. [c] Doubly degenerated modes. [d] Inactive modes.

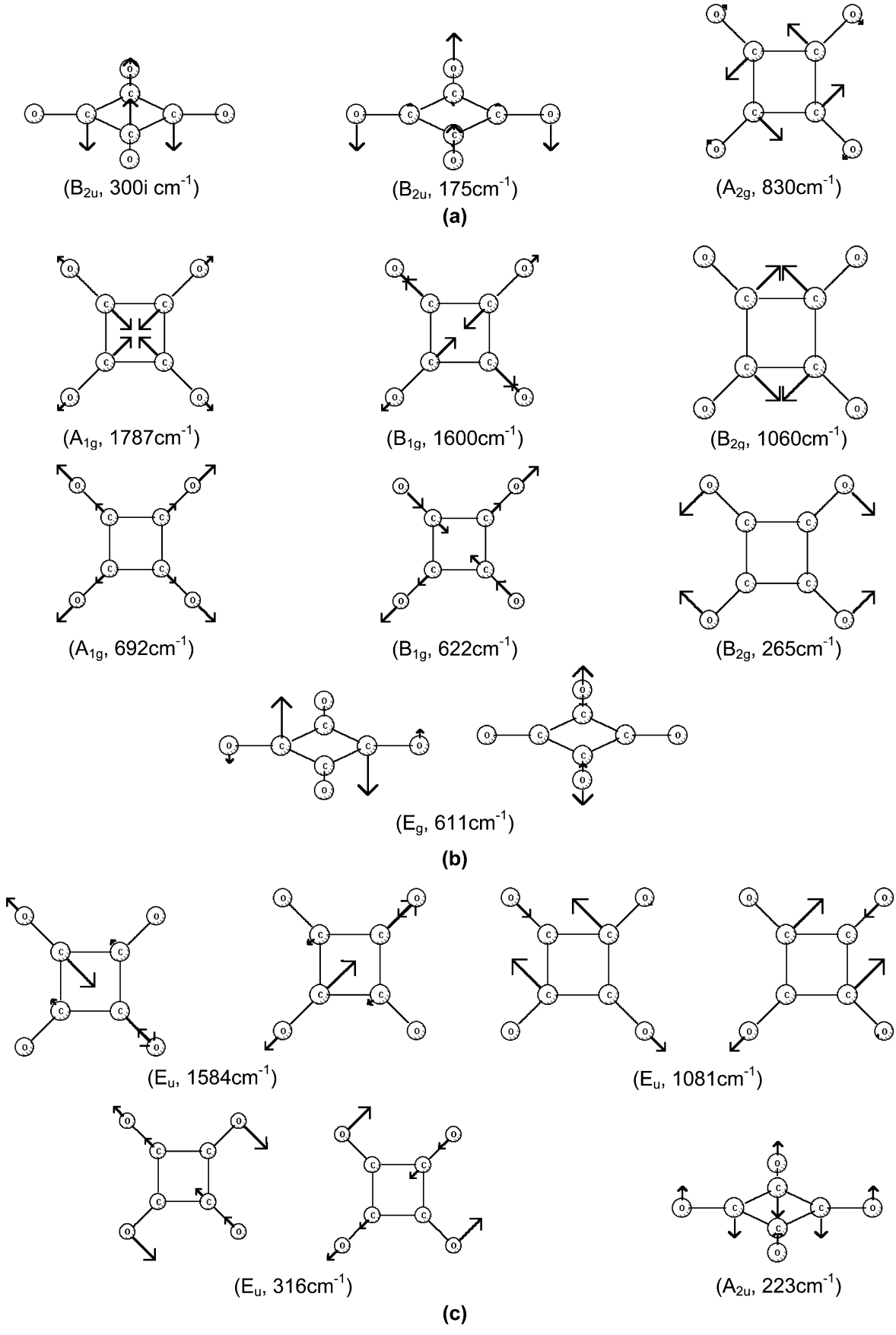

Fig. 2 Representation of the vibrational modes calculated at MP2/6-31+G(d). (a) inative modes. (b) Raman active modes. (c) Infrared active modes.

include the counter-ion effect on the structure and electronic properties of the squarate ion, two complexed forms with stoichiometry $[Li_2(C_4O_4)]$ were proposed (Fig. 3). In the complexed form A (also called *cis*) the squarate ion acts as a bis-bidentated ligand, with the lithium atoms sharing a common oxygen atom. In the form B (also called *trans*) the squarate also acts as bis-bidentated ligand, but with the lithium atoms lying in opposite sides of the ring. Both structures were fully

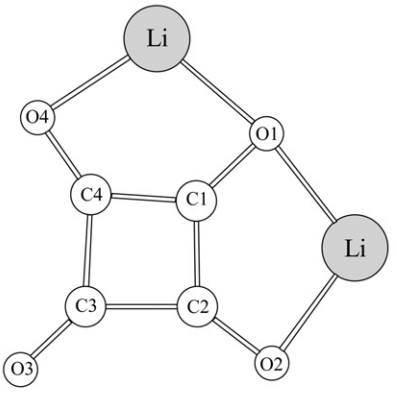

form A (*cis*)

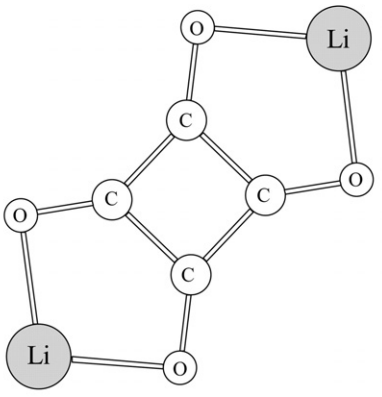

form B (*trans*)

Fig. 3 MP2/6-31+G(d) optimized geometries for the A and B forms of the $[Li_2(C_4O_4)]$ complex.

optimized at MP2/6-31+G(d) level. The energy difference was 8.24 kcal mol^{-1} favoring the form B. However, the dipole moment of the *cis* form (10.46 D) is larger than that calculated for the *trans* form (0.018 D). This should favor the *cis* form in aqueous solution due to electrostatic interactions. Considering the complex with the counter-ion Li^+, the calculated electronic transitions were (in nm/*f*): 316/0.5, 269/0.4 (form A) and 320/0.6, 314/0.5 (form B) assigned to HOMO → LUMO and HOMO → LUMO + 1 for both structures. By comparing with the values for the free anion (357 nm), the HOMO → LUMO transition undergoes a blue shift of 41 nm and the HOMO → LUMO + 1 a corresponding shift of 88 nm for the complexed form A and 37 and 47 nm respectively for the isomer B. As is expected for the squarate anion, the absorption bands should be close to 300 nm.[13] This shows that the Li^+ ions, coordinated either on form A or form B might play an important role in calculating the electronic spectrum of this molecule. Similar conclusions were obtained from our previous papers relative to croconate[20] and deltate[21] derivatives. However in these studies the calculated electronic spectrum of the *cis* form (A) was in better agreement with the experimental finding.

In order to analyse the effect of the type of the counter-ion on the electronic spectrum of the squarate ion we investigated complexed compounds with Na^+ and K^+. Only the *cis* form (A) was considered based on our previous results for the croconate and deltate anions.[20–22] The optimized structural parameters are reported in Table 4. As can be observed in Table 4 a systematic increasing of the M–O bond lengths is observed with the increase of ion size (Li^+, Na^+, K^+). The C–O bonds are shorter for larger ions and a significant decreasing of the O–M–O bond angle is observed from 106° (Li^+) to 79° (K^+).

Table 4 Structural parameters[a] calculated for the complexed compounds *cis*-$[M_2(C_4O_4)]$ in gas phase at MP2/6-31+G(d) level

	Metal ion Li^+	Na^+	K^+
M–O(1)	1.972	2.296	2.601
M–O(4)	1.939	2.261	2.539
C(1)–O(1)	1.326	1.321	1.314
C(4)–O(4)	1.274	1.271	1.269
C(1)–C(4)	1.429	1.447	1.460
C(3)–C(4)	1.529	1.515	1.504
O(1)–M–O(4)	106.0	89.5	78.6

[a] Bond lengths in Å and bond angle in degrees. The numbering scheme is represented in Fig. 3.

The absorption bands for the *cis*-$[Na_2(C_4O_4)]$ and *cis*-$[K_2(C_4O_4)]$ complexes were calculated in gas phase giving transitions close to the *cis*-$[Li_2(C_4O_4)]$ (Table 5). From the values in Table 5 it can be noted that the electronic spectra present the same overall profile for the complexed forms involving distinct counter-ions, predicting two absorption bands close to 310 and 280 nm. This hypothesis was discussed by experimentalists in ref. 39 and briefly considered by us in the reply published as ref. 22. The results obtained in the present paper support our previous conclusions that in order to reproduce the observed electronic spectrum of oxocarbons the counter-ion should be explicitly included, the type of counter-ions being less important.

Electronic spectrum in aqueous solution

Initially we discuss separately the hydrogen bonds between the squarate anion and water molecules. Fig. 4a shows the radial distribution functions (RDF) for the oxygens of the squarate ion and water ($g_{O–O}(r)$, $g_{O–H}(r)$). As can be seen there is a hydrogen bond peak on the $g_{O–O}(r)$ that starts at 2.35 Å and goes up to 3.25 Å. Integration of this peak gives about four water molecules. In the 75 uncorrelated MC configurations, we found a total of 592 hydrogen bonds, giving 8 hydrogen bonds for each configuration. The molecules involved in hydrogen bonds were selected according to the geometric criterion of $r_{OO} \leqslant 4.0$Å and $\angle$ HOO $\leqslant 30°$. Analyzing the $g_{O–H}(r)$ a hydrogen bond peak starting at 1.45 Å up to 2.45 Å is observed. Integration of this peak gives about 2 water molecules on average for each oxygen atom. This is in accordance with the analysis over the 75 uncorrelated configurations. It is important to refer to our previous papers[20–22] on the analysis of the solution structure of croconate and deltate anions. In these papers we showed that each oxygen atom in the oxocarbon derivative is also involved in two hydrogen bonds with water molecules.

In Table 6 the data were organized according to the occurrence of configurations with distinct number of hydrogen

Table 5 Electronic transitions calculated for the *cis*-$[M_2(C_4O_4)]$ (M = Li^+, Na^+ and K^+) using the INDO/CIS method. The MP2/6-31+G(d) gas phase optimized geometries were used. Oscillator strength is in brackets

	Electronic transitions/nm [*f*]	
	HOMO → LUMO	HOMO → LUMO + 1
$[Li_2(C_4O_4)]$	316[0.5]	269[0.4]
$[Na_2(C_4O_4)]$	307[0.5]	280[0.4]
$[K_2(C_4O_4)]$	305[0.6]	275[0.6]

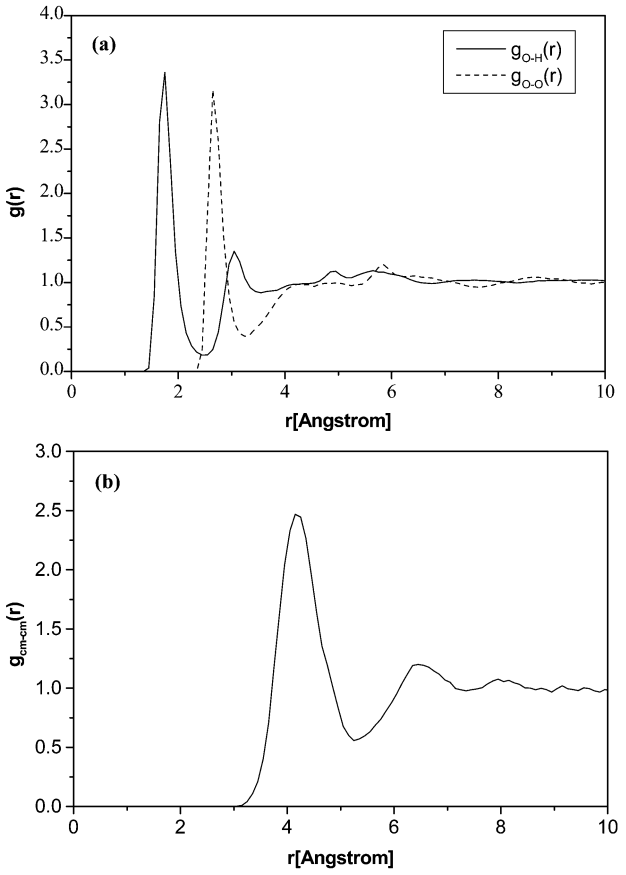

Fig. 4 Radial distribution functions obtained from the MC simulation for the $(C_4O_4)^{2-}$ ion in water (a) O–O and O–H (b) cm–cm.

bonds (NHB). We found that 70% of the selected configurations present 7–9 hydrogen bonds, being the configuration with 7 HB more abundant. As shown in Table 6, a blue shift of both transitions in the electronic spectrum is observed with the increase of the number of the hydrogen bonds.

In the next step we analyze the overall solvent effect on the electronic spectrum of the free squarate ion. The solvation shells were defined from the RDF considering the center of mass (cm) of the solute and solvent molecules ($g_{cm-cm}(r)$). The $g_{cm-cm}(r)$ calculated for the squarate ion in water solution is depicted in Fig. 4b, where two solvation shells are easily distinguished. The first solvation shell was taken from 3.05 Å to 5.25 Å and the second one finished at 7.35 Å. After the spherical integration of the $g_{cm-cm}(r)$ over the corresponding intervals, it was found 20 and 53 water molecules in the first and second solvation shells respectively. According to our previous analysis for the croconate[20] and deltate ions,[21] when the solvent is explicitly included, the HOMO → LUMO and HOMO → LUMO + 1 transitions remains unaltered up to the third solvation shell. So, for the squarate compound we performed the electronic spectrum calculations considering only the addition of the first solvation shell (20 water molecules). The results show that the interaction of the squarate ion with the solvent shifts the absorption bands to the blue region of an amount of 6 nm (HOMO → LUMO) and 11 nm (HOMO → LUMO + 1).

In the last part of this study, we analyzed the combined effects of the counter-ion and solvent on the electronic spectrum of the squarate anion. As was observed in the gas phase analysis, the effect of the counter-ion on the electronic spectrum is non-sensitive to the type of the counter-ion within the series Li^+, Na^+ and K^+, and so we decided to keep the lithium ion, once it was considered in our previous results.[20,21]

As was observed in the gas phase, the coordination of the Li^+ cations in the form A (*cis*) splits the squarate absorption band (357 nm) into two blue shifted absortions, centered at 316 and 269 nm and in form B (*trans*) the absorption bands were found at 320 and 314 nm. In the present study both structures were selected for the MC simulation. The simulation protocol was the same as used for the free $(C_4O_4)^{2-}$ anion described in the methodology section. The σ and ε parameters for the Li^+ ion were taken from the OPLS force field and the atomic charges calculated using the ChelpG procedure at the MP2/6-31+G(d) level of theory. The complete set of parameters used for the structures A and B are included in Table 1. In Fig. 5 the RDF for the Li^+ ion and the oxygen from water, $g_{Li-O}(r)$, are depicted. The narrow peak close to 2 Å in the $g_{Li-O}(r)$ function indicates that the water molecules are strongly bounded to the Li^+ ion. From the $g_{Li-O}(r)$ represented in Fig. 5 it can be seen that there is a peak that starts at 1.85 Å and goes up to 2.75 Å for both forms. Spherical integration of this peak gives two water molecules per lithium atom. The

Table 6 Hydrogen bond analysis and electronic transitions calculated for the $(C_4O_4)^{2-}$ ion in gas phase and water solution. Oscillator strength in brackets

			Electronic transitions/nm [*f*]	
			HOMO → LUMO	HOMO → LUMO + 1
Gas phase			357[0.5]	357[0.5]
Hydrogen bonds (HB)[a]				
NHB[b]	Occurrence[c]	NE[d]		
5	1%	82	355[0.51]	345[0.511]
6	12%	90	353[0.51]	346[0.51]
7	33%	98	354[0.50]	343[0.52]
8	20%	106	355[0.52]	345[0.52]
9	17%	114	354[0.52]	347[0.51]
10	15%	122	353[0.52]	345[0.52]
11	1%	130	349[0.53]	348[0.53]
$[C_4O_4(H_2O)_{20}]^{2-}$		202	351[0.52]	346[0.53]

[a] The water molecules involved in hydrogen bonds were selected according to the geometric criterion of $r_{OO} \leqslant 4.0$ Å and $\angle HOO \leqslant 30°$. [b] Number of hydrogen bonds present in the configurations selected from the MC simulation. [c] The occurrence of hydrogen bonds was calculated relative to the total number of hydrogen bonds (592) on the 75 uncorrelated configurations. [d] Number of valence electrons explicitly included in the quantum mechanical calculations.

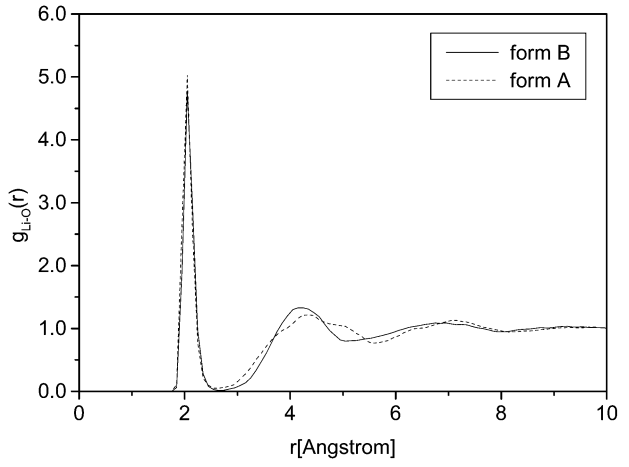

Fig. 5 Representation of the radial distribution functions $g_{Li-O}(r)$ obtained from the MC simulation for the $[Li_2(C_3O_3)]$ complex in the forms A and B.

representations of the supermolecules are depicted in Fig. 6. As was done for the free squarate, the hydrogen bond effects were analyzed separately. In the 75 MC configurations a total of 219 hydrogen bonds were found for the form A and 171 for the isomer B, giving 3 and 2 hydrogen bonds in each configuration, respectively. The larger NHB observed in form A can be attributed to the free oxygen atom in the *cis* complex. As can be observed in Table 7, the maximum numbers of hydrogen bonds found were six (A) and five (B), being the configurations with three and two hydrogen bonds more abundant. Considering only the water molecules that are involved in hydrogen bonds with the solute, a blue shift was observed from 316 to 312 nm (HOMO → LUMO) and 269 to 266 nm (HOMO → LUMO + 1) for structure A and from 320 to 313 (HOMO → LUMO) and 314 to 312 (HOMO → LUMO + 1) for form B. In general the transitions calculated for the form B are more intense.

In order to analyze the effect of additional solvent molecules on the electronic spectrum of squarate, we included water molecules up to the first solvation shell defined from the RDFs considering the center of mass (cm) of the solute and solvent molecules ($g_{cm-cm}(r)$). The $g_{cm-cm}(r)$ calculated for the *cis* and *trans*-$[Li_2(C_4O_4)]$ complexes in water solution are depicted in Fig. 7, where two solvation shells are easily distinguished. The first solvation shell was taken from 2.95 Å to 5.75 Å and the second one finished at 7.95 Å for structure A. After the spherical integration of the $g_{cm-cm}(r)$ over the corresponding intervals, it was found 23 and 68 water molecules in the first and second solvation shells respectively. For the *trans*-form (B), two solvation shells are also easily distinguished. The first one was taken from 3.05 to 5.65 Å and the second one finished at 7.85 Å. The total of solvent molecule on each solvation shell was 21 and 63 respectively. The electronic transitions calculated considering the first solvation shell are reported in Table 7. The result obtained for the cluster *cis*-$[Li_2(C_4O_4)(H_2O)_{23}]$ were 314 and 285 nm (Table 7) and for the *trans*-$[Li_2(C_4O_4)(H_2O)_{21}]$ were 323 and 312 nm. These are close to the values found considering only configurations with few hydrogen bonds. Since electronic transitions are expected close to 300 nm for the squarate anion, our results suggest that the experimental electronic spectrum of that molecule in solution can be reproduced by including the counter-ions and solvent effects. However for the squarate ion the electronic spectrum obtained for the *trans* form is also in agreement with experimental data.

Conclusions

In the present work structure and spectroscopic properties of the squarate ion were analyzed in the gas phase and aqueous

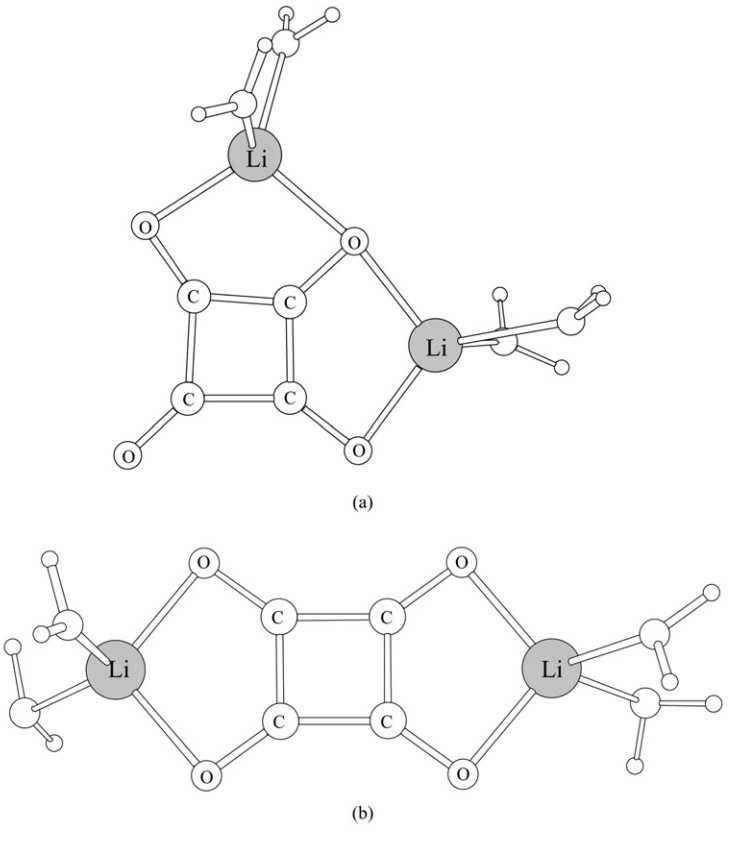

Fig. 6 Supermolecules obtained from the Monte Carlo simulations for the $[Li_2(C_4O_4)]$ complex in the forms A (*cis*) (6a) and B (*trans*) (6b).

Table 7 Hydrogen bond analysis and electronic transitions calculated in gas phase and water solution for the $[Li_2(C_4O_4)]$ complexes in the forms A and B. Oscillator strength in brackets

		Form A (*cis*)			Form B (*trans*)	
		HOMO → LUMO	HOMO → LUMO + 1		HOMO → LUMO	HOMO → LUMO + 1
Gas phase		316[0.5]	269[0.4]		320[0.6]	314[0.5]
NHB[a b c]						
1	15%	315[0.46]	269[0.42]	17%	316[0.60]	314[0.52]
2	24%	314[0.46]	268[0.42]	40%	315[0.58]	312[0.52]
3	31%	313[0.47]	266[0.40]	27%	315[0.58]	312[0.53]
4	17%	313[0.47]	267[0.43]	9%	314[0.57]	311[0.55]
5	12%	313[0.48]	266[0.45]	1%	313[0.50]	312[0.58]
6	1%	312[0.49]	266[0.46]	—	—	—
$[Li_2(C_4O_4)(H_2O)_n]$[e]		314[0.52]	285[0.44]		323[0.54]	312[0.60]

[a] Number of hydrogen bonds presented in the configurations selected from the MC simulation. [b] The water molecules involved in hydrogen bonds were selected according to the geometric criterion of $r_{OO} \leqslant 4.0$ Å and $\angle HOO \leqslant 30°$. [c] The occurrence of hydrogen bonds was calculated relative to the total number of hydrogen bonds (219) for form A and (171) for form B on the 75 uncorrelated configurations. [d] The optimized structures of the complexes $[Li_2(C_4O_4)]$ (forms A and B) are depicted in Fig. 3. [e] $n = 23$ (form A) and $n = 21$ (form B).

solution using theoretical quantum mechanical *ab initio* methods and a sequential Monte Carlo/quantum mechanical approach. The vibrational spectra (infrared and Raman) were calculated in the gas phase at the Møller–Plesset second order perturbation theory (MP2) level, employing standard split-valence basis-sets with inclusion of polarization and diffuse functions on the O and C atoms. Although the geometry was non sensitive to the level of theory used, the vibrational analysis showed an interesting result with an imaginary frequency found at 300i cm^{-1} for the B_{2u} mode when diffuse functions were included in the basis-set (MP2/6-31+G(d)). It becomes real with the inclusion of two sets of d polarization functions on the 6-31+G basis set (91 cm^{-1}), showing that the quality of the basis set plays an important role for the calculation of low frequency vibrational modes.

The calculated electronic spectrum of the squarate ion in the gas phase presented two degenerated transitions at 357 nm. The inclusion of the counter-ion (Li^+) coordinated to the oxocarbon splits and shifts the transitions to the blue region, calculated at 316 and 269 nm. The type of counter ion was found to be less important than the effect itself. Transitions centered in the range of 305–316 nm and 275–269 nm were calculated for complexes with Li^+, Na^+ and K^+.

The combined solvent and counter-ion effects on the electronic spectrum of the squarate anion were analyzed in the last part of the paper. Only the Li^+ ion was considered coordinated to the oxocarbon in the *cis* and *trans* forms. The results were 314 and 285 nm (*cis*) and 323 and 312 nm (*trans*). As we know the experimental electronic spectrum for the squarate derivative has not been reported so far, however following the behavior observed for the oxocarbon series, two absorption bands close to 300 nm could be expected for the $(C_4O_4)^{2-}$ ion, which is in agreement with the values found in this work considering the solvent and the counter-ion effects.

The general conclusion from this study is that in order to reproduce the experimental electronic spectrum of the oxocarbons in solution, we must take into account the combined effects of the solvent and the counter-ion, giving support to our previous results on the oxocarbon series. Finally, it is important to point out that we are not neglecting the role played by the Jahn–Teller effect in explaining the spectral feature. We are just stating that there may be solvent and counter-ion effects can also be used to justify the experimental finding.

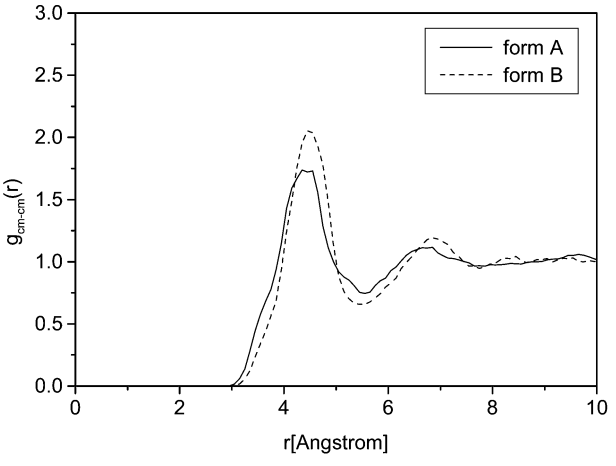

Fig. 7 Radial distribution functions $g_{cm-cm}(r)$ obtained from the MC simulation for the $[Li_2(C_4O_4)]$ complex in the forms A and B.

Acknowledgements

The authors would like to thank the CNPq (Conselho Nacional de Desenvolvimento Científico e Tecnológico) and FAPEMIG (Fundação de Amparo a Pesquisa do Estado de Minas Gerais) by the financial support. The authors also thank the CENAPAD-MG/CO-NAR-UFJF for providing the computational facilities.

References

1 R. West, H. Y. Niu, D. L. Powell and M. V. Evans, *J. Am. Chem. Soc.*, 1960, **82**, 6204.
2 D. Eggerding and R. West, *J. Am. Chem. Soc.*, 1975, **97**, 207.
3 M. Ito and R. West, *J. Am. Chem. Soc.*, 1963, **85**, 2580.
4 R. West and H. Y. Niu, *J. Am. Chem. Soc.*, 1963, **85**, 2586.
5 R. West, J. W. Downing, S. Inagaki and J. Michl, *J. Am. Chem. Soc.*, 1981, **103**, 5073.
6 (*a*) P. S. Santos, J. H. Amaral and L. F. C. de Oliveira, *J. Mol. Struct.*, 1991, **243**, 223; (*b*) L. F. C. de Oliveira, J. G. da Silva Lopes, P. M. V. B. Barone, M. C. C. Ribeiro and P. S. Santos, *J. Mol. Struct. (THEOCHEM)*, 1999, **510**, 97; (*c*) J. G. S. Lopes, L. F. C. de Oliveira and P. S. Santos, *Spectr. Acta Part A*, 2001, **57**, 399.
7 M. D. Glick, G. L. Downs and L. F. Dahl, *Inorg. Chem.*, 1964, **3**, 1712.
8 M. D. Glick and L. F. Dahl, *Inorg. Chem.*, 1966, **5**, 289.

9 F. Dumestre, B. Soula, A. M. Galibert, P. L. Fabre, G. Bernardinelli, B. Donnadieu and P. Castan, *J. Chem. Soc., Dalton. Trans.*, 1998, **24**, 4131.
10 N. S. Gonçalves, P. S. Santos and I. Vencato, *Acta Crystallogr., Sect. C*, 1996, **C52**, 622.
11 J. Aihara, *J. Am. Chem. Soc.*, 1981, **103**, 1633.
12 P. von R. Schleyer, K. Najafian, B. Kiran and H. Jiao, *J. Org. Chem.*, 2000, **65**, 426.
13 M. Takahashi, K. Kaya and M. Ito, *Chem. Phys.*, 1978, **35**, 293.
14 (*a*) G. Seitz and P. Imming, *Chem. Rev.*, 1992, **92**, 1227; (*b*) B. Zhao and M. H. Back, *Can. J. Chem.*, 1992, **70**, 135; (*c*) M. Dory, J. M. André, J. Delhalle and J. O. Morley, *J. Chem. Soc. Faraday. Trans.*, 1994, **16**, 2319; (*d*) P. L. Fabre, F. Dumestre, B. Soula and A. M. Galibert, *Electrochim. Acta*, 2000, **45**, 2697.
15 R. West and D. L. Powell, *J. Am. Chem. Soc.*, 1963, **85**, 2577.
16 L. Farnell, L. Radom and M. A. Vincent, *J. Mol. Struct. (THEOCHEM)*, 1981, **76**, 1.
17 C. Puebla and T. K. Ha, *J. Mol. Struct. (THEOCHEM)*, 1986, **137**, 171.
18 T. K. Ha and C. Puebla, *J. Mol. Struct. (THEOCHEM)*, 1986, **137**, 183.
19 H. Torii and M. Tasumi, *J. Mol. Struct. (THEOCHEM)*, 1995, **334**, 15.
20 G. M. A. Junqueira, W. R. Rocha, W. B. De Almeida and H. F. Dos Santos, *Phys. Chem. Chem. Phys.*, 2001, **3**, 3499.
21 G. M. A. Junqueira, W. R. Rocha, W. B. De Almeida and H. F. Dos Santos, *Phys. Chem. Chem. Phys.*, 2002, **4**, 2517.
22 G. M. A. Junqueira, W. R. Rocha, W. B. De Almeida and H. F. Dos Santos, *Phys. Chem. Chem. Phys.*, 2002, **4**, 2919.
23 (*a*) L. F. C. de Oliveira and P. S. Santos, *J. Mol. Struct.*, 1991, **245**, 215; (*b*) L. F. C. de Oliveira and P. S. Santos, *J. Mol. Struct.*, 1992, **269**, 85; (*c*) H. Torii and M. Tasumi, *J. Mol. Struct. (THEOCHEM)*, 1995, **334**, 15; (*d*) S. G. de Miranda and P. A. M. Vasquez, *J. Braz. Chem. Soc.*, 2002, **13**, 324.
24 M. Spassova, T. Kolev, I. Kanev, D. Jacquemin and B. Champagne, *J. Mol. Struct. (THEOCHEM)*, 2000, **528**, 151.
25 (*a*) G. A. Peterson and M. A. Al-Laham, *J. Chem. Phys.*, 1991, **94**, 6081; (*b*) R. Krishnan, J. S. Binkley, R. Seeger and J. A. Pople, *J. Chem. Phys.*, 1980, **72**, 650; (*c*) M. J. Frisch, J. A. Pople and J. S. Binkley, *J. Chem. Phys.*, 1984, **80**, 3265.
26 (*a*) J. Ridley and M. C. Zerner, *Theor. Chim. Acta.*, 1973, **32**, 111; (*b*) M. C. Zerner, R. Loew, R. F. Kirchner and V. T. Mueller-Westerholf, *J. Am. Chem. Soc.*, 1980, **102**, 589; (*c*) D. Head and M. C. Zerner, *Chem. Phys. Lett.*, 1986, **131**, 359; (*d*) W. D. Edwalds and M. C. Zerner, *Theor. Chim. Acta.*, 1987, **72**, 347.
27 M. P. Allen and D. J. Tildesley, in *Computer Simulation of Liquids*, Oxford University Press, Oxford, 1987.
28 M. Metropolis, M. N. Rosenbluth, A. H. Rosenbluth, A. H. Teller and E. Teller, *J. Chem. Phys.*, 1953, **21**, 1087.
29 *Handbook of Chemistry and Physics*, CRC Press, Boca Raton, FL, 73rd edn., 1992–1993.
30 W. Damm, A. Frontera, J. Tirado-Rives and W. L. Jörgensen, *J. Comput. Chem.*, 1997, **18**, 1995.
31 D. Quinoñero, S. Tomás, A. Frontera, C. Garau, P. Ballester, A. Costa and P. M. Deyá, *Chem. Phys. Lett.*, 2001, **350**, 331.
32 C. M. Breneman and K. B. Wiberg, *J. Comput. Chem.*, 1990, **11**, 361.
33 W. L. Jorgensen, J. Chandrasekhar, J. D. Madura, R. W. Impey and M. L. Klein, *J. Chem. Phys.*, 1983, **79**, 926.
34 K. Coutinho and S. Canuto, *Adv. Quantum Chem.*, 1997, **28**, 89.
35 (*a*) W. R. Rocha, K. Coutinho, W. B. De Almeida and S. Canuto, *Chem. Phys. Lett.*, 2001, **127**, 335; (*b*) K. J. De Almeida, K. Coutinho, W. B. De Almeida, W. R. Rocha and S. Canuto, *Phys. Chem. Chem. Phys.*, 2001, **3**, 1583; (*c*) K. Coutinho and S. Canuto, *J. Chem. Phys.*, 2000, **113**, 9132; (*d*) S. Canuto and K. Coutinho, *Int. J. Quantum Chem.*, 2000, **77**, 192.
36 M. J. Frisch, G. W. Trucks, H. B. Schlegel, G. E. Scuseria, M. A. Robb, J. R. Cheeseman, V. G. Zakrzewski, J. A. Montgomery, Jr., R. E. Stratmann, J. C. Burant, S. Dapprich, J. M. Millam, A. D. Daniels, K. N. Kudin, M. C. Strain, O. Farkas, J. Tomasi, V. Barone, M. Cossi, R. Cammi, B. Mennucci, C. Pomelli, C. Adamo, S. Clifford, J. Ochterski, G. A. Petersson, P. Y. Ayala, Q. Cui, K. Morokuma, D. K. Malick, A. D. Rabuck, K. Raghavachari, J. B. Foresman, J. Cioslowski, J. V. Ortiz, B. B. Stefanov, G. Liu, A. Liashenko, P. Piskorz, I. Komaromi, R. Gomperts, R. L. Martin, D. J. Fox, T. Keith, M. A. Al-Laham, C. Y. Peng, A. Nanayakkara, C. Gonzalez, M. Challacombe, P. M. W. Gill, B. G. Johnson, W. Chen, M. W. Wong, J. L. Andres, M. Head-Gordon, E. S. Replogle and J. A. Pople, *GAUSSIAN 98 (Revision A.6)*, Gaussian, Inc., Pittsburgh, PA, 1998.
37 K. Coutinho and S. Canuto, *DICE: A Monte Carlo Program for Liquid Simulation*, University of São Paulo, 1997.
38 R. West, D. Eggerding, J. Perkins, D. Handy and E. C. Tuazon, *J. Am. Chem. Soc.*, 1979, **101**, 1710.
39 M. C. C. Ribeiro and A. O. Cavalcante, *Phys. Chem. Chem. Phys.*, 2002, **4**, 2917.
40 W. M. Macintyre and M. S. Werkema, *J. Chem. Phys.*, 1964, **42**, 3563.